BRL

END

DATE
FILMED
7-77

1·0   2·8   2·5

3·15   2·2

3·5

1·1   4·0   2·0

4·5   1·8

1·25   1·4   1·6

NATIONAL BUREAU OF STANDARDS
MICROCOPY RESOLUTION TEST CHART

BRL

AD

CONTRACT REPORT NO. 338

THREE-DIMENSIONAL COMPUTATIONS ON
PENETRATOR-TARGET INTERACTIONS

Prepared by

Computer Code Consultants
527 Glencrest Drive
Solana Beach, CA 92075

D D C

JUN 29 1977

C

April 1977

USA ARMAMENT RESEARCH AND DEVELOPMENT COMMAND
USA BALLISTIC RESEARCH LABORATORY
ABERDEEN PROVING GROUND, MARYLAND

REPORT DOCUMENTATION PAGE		READ INSTRUCTIONS BEFORE COMPLETING FORM
1. REPORT NUMBER BRL Contract Report No. 338	2. GOVT ACCESSION NO.	3. RECIPIENT'S CATALOG NUMBER
4. TITLE (and Subtitle) Three-Dimensional Computations on Penetrator-Target Interactions		5. TYPE OF REPORT & PERIOD COVERED BRL Contractor Report Nov 1974 - Dec 1975
		6. PERFORMING ORG. REPORT NUMBER
7. AUTHOR(s) Wallace E. Johnson		8. CONTRACT OR GRANT NUMBER(s) DAAD05-75-C-0738
9. PERFORMING ORGANIZATION NAME AND ADDRESS Computer Code Consultants 527 Glencrest Drive Solana Beach, California 92075		10. PROGRAM ELEMENT, PROJECT, TASK AREA & WORK UNIT NUMBERS 61102A 1T161102A33 002AJ
11. CONTROLLING OFFICE NAME AND ADDRESS USA Ballistic Research Laboratory Aberdeen Proving Ground, Maryland 21005		12. REPORT DATE APR 1977
		13. NUMBER OF PAGES 62
14. MONITORING AGENCY NAME & ADDRESS(if different from Controlling Office)		15. SECURITY CLASS. (of this report) Unclassified
		15a. DECLASSIFICATION/DOWNGRADING SCHEDULE

16. DISTRIBUTION STATEMENT (of this Report)

Approved for public release; distribution unlimited.

17. DISTRIBUTION STATEMENT (of the abstract entered in Block 20, if different from Report)

18. SUPPLEMENTARY NOTES

19. KEY WORDS (Continue on reverse side if necessary and identify by block number)

Jet Penetration
Hypervelocity Impact
Hydrodynamic Code
Eulerian Code
Two-dimensional Code

Impact Mechanics
Shaped Charge Jets
Fuel Impact

20. ABSTRACT (Continue on reverse side if necessary and identify by block number)

The three-dimensional, two-material, rigid-plastic code, TRIDORF, was used to solve penetration calculations of shaped charge jets impacting thin targets at four angles of obliquity. A fuel target interaction with a shaped charge jet was solved by using the two-dimensional DORF code and the TRIDORF code.

DD FORM 1473 1 JAN 73   EDITION OF 1 NOV 65 IS OBSOLETE

TABLE OF CONTENTS

iii

LIST OF ILLUSTRATIONS

LIST OF ILLUSTRATIONS (Continued)

I.   INTRODUCTION

For several years the Ballistics Research Laboratories, using computer codes, have been investigating the phenomena associated with the penetration by a shaped-charged jet into vehicle armor. The purpose of these investigations has been to provide an armor configuration that is light in weight but effective against shaped-charged jets.

The computer codes presently available can numerically solve problems of normal or zero obliquity impact. For plane strain, planes of non-zero obliquity can be solved using X-Y versions of Eulerian codes. There are certain unique phenomena which occur during oblique impact; consequently, a three-dimensional model of the penetration process is required to investigate in detail the phenomena associated with oblique impact.

TRIDORF[2] is capable of performing these oblique impact calculations. TRIDORF is a two-material version of TRIOIL[1] with a rigid-perfectly plastic strength formulation. The description of the TRIDORF code is reported in Section II. A normal impact has been checked against the DORF[3] code (two-dimensional) and is reported in Section III.

A series of four oblique impact calculations (copper jet impacting a steel plate) have been solved using the TRIDORF code and are reported in Section IV. In addition, three oblique impact calculations (plexiglass spheres impacting a plexiglass plate) performed for the Naval Research Laboratory are reported in Section IV.

A fuel target configuration has been calculated with a two-dimensional model (DORF) transferring over to the three-dimensional model (TRIDORF) when the stress wave (generated by the rigid jet) reaches the walls of the cylinder.

---

[1] Johnson, W. E., "TRIOIL - A Three-Dimensional Version of the OIL Code," GAMD-7310, General Atomic, June 1967.

[2] Johnson, W. E., "TRIDORF - A Two-Material Version of the TRIOIL Code with Strength," Computer Code Consultants, to be published.

[3] Johnson W. E., "Code Correlation Study," Technical Report No. AFWL-TR-70-144, April 1971; and Johnson, W. E., "Development and Application of Computer Programs to Hypervelocity Impact," 3SR-749, Systems, Science and Software, July 1971.

The results of these calculations are described in Section V. The code modifications, for both DORF and TRIDORF, required for these tasks are described in Section VII.

A multi-material normal impact calculation has been solved using the DORF[3] code and is reported in Section VI. A splitting (a method of fractional steps, where one can replace a complicated multi-dimensional problem by a succession of simpler one-dimensional ones) version of the OIL[4] code and techniques to eliminate the conventional "if" tests from Eulerian formulations are described in Section VII.

II. DESCRIPTION OF NUMERICAL TECHNIQUES

The TRIOIL[1] code has been modified to treat two materials, and a rigid-perfectly plastic strength model has been included. A routine to move massless tracer particles has also been incorporated into the code. This version is called TRIDORF[2] and is in the final state of documentation. The basic difference equations for the Lagrangian phase, the convective phase and the strength phase are listed below. Familiarity with the OIL[4] family of codes is assumed.

---

[4]Johnson, W. E., "OIL - A Continuous Two-Dimensional Eulerian Hydrodynamic Code," GAMD-5580, General Atomic, June 1965.

2

A. Difference Equations For Phase 1 (Lagrangian Phase)

The Eulerian equations we wish to solve are the following:

$$\frac{\partial \rho}{\partial t} + \nabla \cdot (\rho \vec{u}) = 0 \tag{1}$$

$$\frac{\partial \rho \vec{u}}{\partial t} + \vec{u} \cdot \nabla \rho \vec{u} = -\nabla P \tag{2}$$

$$\frac{\partial \rho E}{\partial t} + \nabla \cdot (\rho E \vec{u}) = -\nabla \cdot (P \vec{u}) \tag{3}$$

Equation 1 is the conservation of mass equation, Equation 2 is the conservation of momentum equation, and Equation 3 is the conservation of energy equation.

The second terms on the left side of Equations 1, 2 and 3 are temporarily dropped. Their contributions are later approximated when we move mass across cell boundaries. Rewriting Equations 2 and 3 in cartesian coordinates results in Equations 4, 5, 6 and 7.

$$\rho \frac{\partial u}{\partial t} = - \frac{\partial P}{\partial x} \tag{4}$$

$$\rho \frac{\partial v}{\partial t} = - \frac{\partial P}{\partial y} \tag{5}$$

$$\rho \frac{\partial w}{\partial t} = - \frac{\partial P}{\partial z} \tag{6}$$

$$\rho \frac{\partial E}{\partial t} = - \frac{\partial (Pu)}{\partial x} - \frac{\partial (Pv)}{\partial y} - \frac{\partial (Pw)}{\partial z} \tag{7}$$

3

ρ = density of cell L, g/cm^3

x = x coordinate, cm

y = y coordinate, cm

z = z coordinate, cm

u = x component of velocity, cm/shake
(1 shake = 10^{-8} sec)

v = y component of velocity, cm/shake

w = z component of velocity, cm/shake

P = $f(\rho,Q)$ from the equation of state
= material pressure, jerks/cm^3
(1 jerk = 10^{16} ergs)

E = total specific energy, jerks/g

t = time, shakes

Q = specific internal energy, jerks/g.

Rewriting Equation 7,

$$\rho \frac{\partial E}{\partial t} = - \frac{\partial (Pu)}{\partial x} - \frac{\partial (Pv)}{\partial y} - \frac{\partial (Pw)}{\partial z}$$

or, substituting for the total specific energy,

$$\rho \frac{\partial}{\partial t} \left[Q + \frac{1}{2}\left(u^2 + v^2 + w^2\right) \right] = - \frac{\partial (Pu)}{\partial x} - \frac{\partial (Pv)}{\partial y} - \frac{\partial (Pw)}{\partial z}$$

and differentiating,

$$\rho \frac{\partial Q}{\partial t} + \rho u \frac{\partial u}{\partial t} + \rho v \frac{\partial v}{\partial t} + \rho w \frac{\partial w}{\partial t} = -P \frac{\partial u}{\partial x} - u \frac{\partial P}{\partial x}$$

$$- P \frac{\partial v}{\partial y} - v \frac{\partial P}{\partial y} - P \frac{\partial w}{\partial z} - w \frac{\partial P}{\partial z} ,$$

4

But

$$\rho \, \frac{\partial u}{\partial t} \; = \; - \; \frac{\partial P}{\partial x} \quad \text{and} \quad \rho \, \frac{\partial v}{\partial t} \; = \; - \; \frac{\partial P}{\partial y} \quad \text{and} \quad \rho \, \frac{\partial w}{\partial t} \; = \; - \; \frac{\partial P}{\partial z} ,$$

thus

$$\rho \, \frac{\partial Q}{\partial t} \; = \; -P \left[\frac{\partial u}{\partial x} \; + \; \frac{\partial v}{\partial y} \; + \; \frac{\partial w}{\partial z} \right] \; . \tag{8}$$
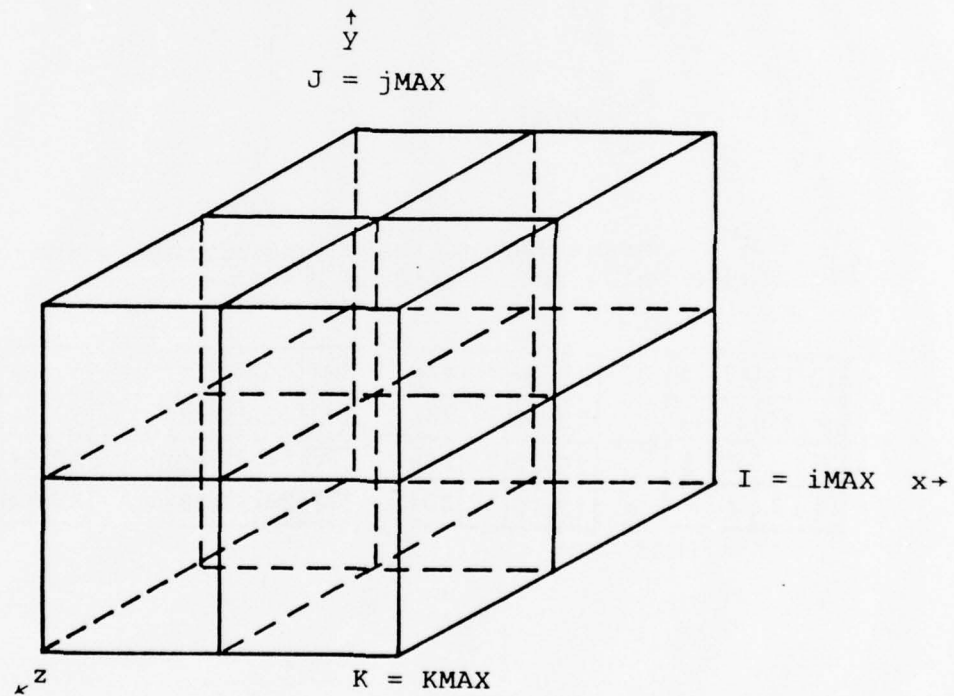
A VIEW OF A THREE-DIMENSIONAL GRID

5

The ρ, u, v, w, P, E and Q are all cell-centered quantities with the cell index L, which is defined as

$$L = (J-1) \ iMAX + I + (K-1) \ iXMAX$$
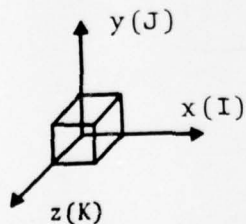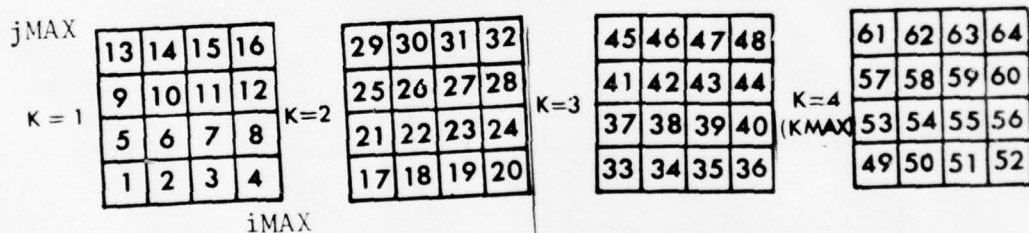
where   iXMAX = (iMAX)(jMAX).

Also,

$$x(I) = \sum_{i=1}^{I} \Delta x(i)$$

$$y(J) = \sum_{j=1}^{J} \Delta y(j)$$

$$z(K) = \sum_{k=1}^{K} \Delta Z(k) \quad .$$

The L storage for the cell quantities is indicated in the figure below for a grid of $4 \times 4 \times 4$.

The x-momentum equation (4) becomes, in difference form,

$$\rho_L^n \left(\frac{\tilde{u}_L - u_L^n}{\Delta t} \right) = \frac{P_{L-1}^n - P_{L+1}^n}{2 \Delta x(I)} \quad .$$

The y-momentum equation (5) becomes, in difference form,

$$\rho_L^n \left(\frac{\tilde{v}_L - v_L^n}{\Delta t} \right) = \frac{P_{L-iMAX}^n - P_{L+iMAX}^n}{2 \Delta y(J)} \quad .$$

The z-momentum equation (6) becomes, in difference form,

$$\rho_L^n \left(\frac{\tilde{w}_L - w_L^n}{\Delta t} \right) = \frac{P_{L-iXMAX}^n - P_{L+iXMAX}^n}{2 \Delta z(K)} \quad .$$

The ($\tilde{\ }$) refers to the velocities at the completion of Phase 1 (not at cycle n+1, since we have neglected the transport terms at this stage). Here the acceleration of cell L is seen to depend only on the pressures in the neighboring cells and not that of L. Defining pressures at interfaces,

$$PL^n = \frac{P_{L-1}^n + P_L^n}{2} \qquad\qquad PBLO^n = \frac{P_{L-iMAX}^n + P_L^n}{2}$$

$$PRR^n = \frac{P_L^n + P_{L+1}^n}{2} \qquad\qquad PABOVE^n = \frac{P_L^n + P_{L+iMAX}^n}{2}$$

7

$$PBIND^n = \frac{P^n_{L-iXMAX} + P^n_L}{2}$$

$$PZR^n = \frac{P^n_{L+iXMAX} + P^n_L}{2} \quad .$$

Substitution of these interface pressures into the three-momentum equations results in

$$\tilde{u}_L - u^n_L = \frac{\Delta t}{\rho^n_L}\left[\frac{PL^n - PRR^n}{\Delta x(I)}\right]$$

$$\tilde{v}_L - v^n_L = \frac{\Delta t}{\rho^n_L}\left[\frac{PBLO^n - PABOVE^n}{\Delta y(J)}\right]$$

$$\tilde{w}_L - w^n_L = \frac{\Delta t}{\rho^n_L}\left[\frac{PBIND^n - PZR^n}{\Delta z(K)}\right]$$

where the usual tilda ($\tilde{\ }$) designates the new velocities (not at cycle n+1), since we have temporarily dropped the transport terms.

The specific internal energy equation becomes

$$\frac{\Delta Q}{\Delta t} = -P^n_L\left[\frac{v^{n+1/2}_{L-iMAX} - v^{n+1/2}_{L+iMAX}}{2\Delta y(J)} + \frac{u^{n+1/2}_{L-1} - u^{n+1/2}_{L+1}}{2\Delta x(I)}\right.$$

$$\left. + \frac{w^{n+1/2}_{L-iXMAX} - w^{n+1/2}_{L+iXMAX}}{2\Delta z(K)}\right]\bigg/MASS$$

$$MASS = AMX(L) + AMD(L)$$

where Q = specific internal energy, AMX = X mass of cell, gm and AMD = · mass of cell, gm. The reason for the velocities at time (n+1/2) can be seen from energy con-servation considerations. Defining

$$u_L^{n+1/2} = \frac{u_L^n + \tilde{u}_L}{2}$$

$$v_L^{n+1/2} = \frac{v_L^n + \tilde{v}_L}{2}$$

$$w_L^{n+1/2} = \frac{w_L^n + \tilde{w}_L}{2}$$

and

$$VBLO = \frac{v_L + v_{L-iMAX}}{2}$$

$$VABOVE = \frac{v_L + v_{L+iMAX}}{2}$$

$$UL = \frac{U_L + U_{L-1}}{2}$$

$$URR = \frac{U_L + U_{L+1}}{2}$$

$$UBIND = \frac{W_L + W_{L-iXMAX}}{2}$$

$$WZR = \frac{W_L + W_{L+iXMAX}}{2}$$

then

9

$$\left(\frac{\Delta Q}{\Delta t}\right) = P_L^n \left[\frac{VBLO^n + VB\tilde{L}O}{2\Delta y(J)} - \frac{VABOVE^n + VA\tilde{B}OVE}{2\Delta y(J)} + \frac{UL^n + \tilde{U}L}{2\Delta x(I)} \right.$$

$$\left. - \frac{URR^n + U\tilde{R}R}{2\Delta x(I)} + \frac{UBIND^n + UB\tilde{I}ND}{2\Delta z(K)} - \frac{WZR^n + W\tilde{Z}R}{2\Delta z(K)} \right] \bigg/ MAS\dot{S}$$

The solution of the momentum equations are very straightforward; however, the solution to the energy equation requires the old and new velocities. Two passes are made through the routine: The first pass formulates the interface velocities for the work term contribution to the internal energy before integrating the momentum equations (since we have allowed only one array per velocity component), and the second pass bypasses the momentum equations and only computes the new interface velocities for their contribution to the work term.

The change in specific internal energy for each material is assumed to be proportional to the fractional volume of each

$$\Delta Q_x = \Delta Q f / M_x$$

and

$$\Delta Q_. = \Delta Q (1-f) / M_.$$

where (x) and (·) refer to the two different materials, x and dot respectively, and f is the fraction of the total cell volume occupied by (x) material. The factor, f, is calculated from the equation of state, where we iterate on the densities until the pressures of each material are the same.

10

B. Difference Equations For Phase 2 (Convective Phase)

The Eulerian equations we wish to solve are the following:

$$\frac{\partial \rho}{\partial t} = -\nabla \cdot (\rho \vec{u}) \tag{9}$$

$$\frac{\partial \rho u}{\partial t} = -\vec{u} \cdot \nabla \rho \vec{u} \tag{10}$$

$$\frac{\partial \rho E}{\partial t} = -\nabla \cdot (\rho E \vec{u}) \tag{11}$$

Rewriting Equation 9, the mass transport equation in finite difference form results in

$$\frac{\rho_L^{n+1} - \rho_L^n}{\Delta t} = \left[\frac{\rho_{J-1}^n \bar{v}_{J-1} - \rho_J^n \bar{v}_J}{\Delta y(J)} + \frac{\rho_{I-1}^n \bar{u}_{I-1} - \rho_I \bar{u}_I}{\Delta x(I)} \right.$$

$$\left. + \frac{\rho_{K-1}^n \bar{w}_{K-1} - \rho_K^n \bar{w}_K}{\Delta Z(K)} \right].$$

The velocities $\bar{v}$, $\bar{u}$ and $\bar{w}$ are average type velocities as described in Reference 1.

Mass, the three components of momentum and the energy across all six sides of the parallelpiped are calculated. By conserving the x, y and z momentum and the total energy, the new velocities are calculated and the new specific internal energy is the difference between the total energy in the cell (after transport) and the new kinetic energy.

For the mass fluxes, we must determine (for a mixed cell) how much of each material to move. Four possible situations concerned with two materials arise.

(1) Material moving from a non-mixed cell to a mixed cell. This presents no difficulty or modification to the transport terms.

EXAMPLE (non-mixed to mixed):

LA ← x and · materials

A_J (cell interface area)
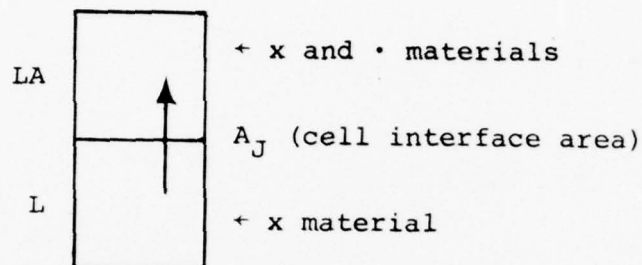
L ← x material
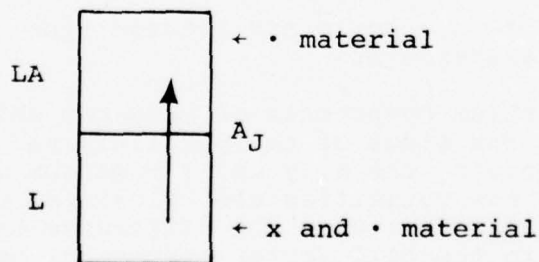
Mass flow is from cell L to cell LA.

$$\Delta M = \rho_L \; \bar{v} \; A_J \; \Delta t$$

$$\Delta M_x = \Delta M$$

$$\Delta M_. = 0$$

where ρ = density of x material in cell L.

(2) From a mixed to a pure cell:

LA ← · material

A_J

L ← x and · material

The flux is positive from cell L to cell LA.

12

The volume of material to move from cell L to cell LA is $\bar{V}\Delta t$ (DX(I) DZ(K)) where $\bar{V}$ is the weighted velocity to use in the mass flux equation. The volume of x material in cell L is VOL, the volume of the dot material is (1-f)VOL.

A. If $\bar{V}\Delta t$ (DX(I) DZ(K)) > (1-f)VOL, let all the dot mass move out, that is, set $\Delta M_. = AMD(L)$. Now the remainder of the volume to move will be assigned to the x flux as follows: We can calculate the x mass to move from conservation of partial volumes,

$$\bar{V}\Delta t(DX(I) \ DZ(K)) = VOL_x + VOL_. = \frac{\Delta M_x}{\rho_x} + (1-f)VOL.$$
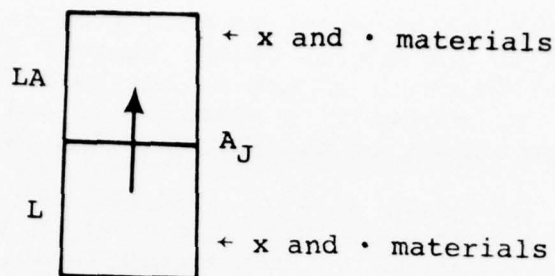
But

$$\rho_x = \frac{AMX(L)}{f \ VOL} ,$$

thus

$$\Delta M_x = [\bar{V} \ \Delta t - (1-f) \ DY(J)] \frac{AMX(L)}{f \ DY(J)}$$

B. If $\bar{V}\Delta t(DX(I) \ DZ(K)) < (1-f)VOL$ then the x mass to move ΔM_X is set to 0 and the dot mass to move $\Delta M_.$ is given by

$$\Delta M_. = \frac{AMD(L)}{(1-f)DY(J)} \ \bar{V} \ \Delta t = \rho\bar{V} \ A\Delta t .$$

(3) Material moving from a mixed cell to a mixed cell requires some modification in the transport terms in order to keep the material interface defined in a single mixed cell.
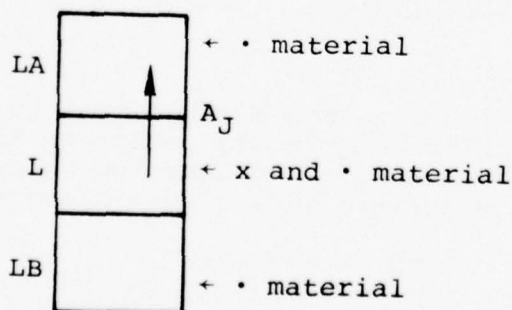
EXAMPLE (mixed to mixed):

13

Mass flow is from cell L to cell LA.
$\Delta M = \rho \bar{V} A_J \Delta t$, where ρ is the total
density of both materials in cell L,
then

$$\Delta M_x = \frac{M_x^L + M_x^{LA}}{M_x^L + M_x^{LA} + M_{\cdot}^L + M_{\cdot}^{LA}} \Delta M$$

$$\Delta M_{\cdot} = \frac{M_{\cdot}^L + M_{\cdot}^{LA}}{M_x^L + M_x^{LA} + M_{\cdot}^L + M_{\cdot}^{LA}} \Delta M$$

(4) From a mixed to a pure cell, with a pure like
     material below — use the mass weighting scheme
     as calculated in situation Number 3.

C. Difference Equations For Phase 3 (Strength Phase)

The Eulerian equations for the rigid-perfectly plastic strength equations are again, dropping the transport terms:

Conservation of Momentum:

$$\rho \frac{\partial u_i}{\partial t} = \sigma_{ij,j}$$

Conservation of Energy:

$$\rho \frac{\partial E}{\partial t} = (\sigma_{ij} u_i), j$$

where E = total energy per gram, internal plus kinetic.

The deviatoric stresses are defined as

$$\sigma_{ij} = B\left(\dot{e}_{ij} - \delta_{ij}\frac{\dot{e}_{aa}}{3}\right) = B \, \dot{\varepsilon}_{ij}$$

where

$$B = \frac{y \sqrt{2}}{\sqrt{\dot{\varepsilon}_{ab} \dot{\varepsilon}_{ab}}} \quad \text{(y is defined on page 22)}$$

$$\dot{e}_{ij} = \left\{ \begin{matrix} \dfrac{\partial u}{\partial x} & \dfrac{1}{2}\left(\dfrac{\partial u}{\partial y} + \dfrac{\partial v}{\partial x}\right) & \dfrac{1}{2}\left(\dfrac{\partial u}{\partial z} + \dfrac{\partial w}{\partial x}\right) \\[2ex] \dfrac{1}{2}\left(\dfrac{\partial v}{\partial x} + \dfrac{\partial u}{\partial y}\right) & \dfrac{\partial v}{\partial y} & \dfrac{1}{2}\left(\dfrac{\partial v}{\partial z} + \dfrac{\partial w}{\partial y}\right) \\[2ex] \dfrac{1}{2}\left(\dfrac{\partial w}{\partial x} + \dfrac{\partial u}{\partial z}\right) & \dfrac{1}{2}\left(\dfrac{\partial w}{\partial y} + \dfrac{\partial v}{\partial z}\right) & \dfrac{\partial w}{\partial z} \end{matrix} \right\}$$

15

$$\dot{\varepsilon}_{ij}\,\dot{\varepsilon}_{ij} = \left(\dot{e}_{ij} - \frac{\delta_{ij}\,\dot{e}_{aa}}{3}\right)^2$$

$$= \left(\frac{\partial u}{\partial x}\right)^2 + \left(\frac{\partial v}{\partial y}\right)^2 + \left(\frac{\partial w}{\partial z}\right)^2 + 2\left[\frac{1}{2}\left(\frac{\partial v}{\partial x} + \frac{\partial u}{\partial y}\right)\right]^2$$

$$+ 2\left[\frac{1}{2}\left(\frac{\partial u}{\partial z} + \frac{\partial w}{\partial x}\right)\right]^2 + 2\left[\frac{1}{2}\left(\frac{\partial v}{\partial z} + \frac{\partial w}{\partial y}\right)\right]^2$$

$$- \frac{1}{3}\left(\frac{\partial u}{\partial x} + \frac{\partial v}{\partial y} + \frac{\partial w}{\partial z}\right)^2$$

$$= \left(\frac{\partial u}{\partial x}\right)^2 + \left(\frac{\partial v}{\partial y}\right)^2 + \left(\frac{\partial w}{\partial z}\right)^2$$

$$- \frac{1}{3}\left[\frac{\partial u}{\partial x} + \frac{\partial v}{\partial y} + \frac{\partial w}{\partial z}\right]^2$$

$$+ \frac{1}{2}\left(\frac{\partial v}{\partial x} + \frac{\partial u}{\partial y}\right)^2 + \frac{1}{2}\left(\frac{\partial u}{\partial z} + \frac{\partial w}{\partial x}\right)^2 + \frac{1}{2}\left(\frac{\partial v}{\partial z} + \frac{\partial w}{\partial y}\right)^2$$

The forces these stresses produce are then simply the stresses multiplied by the area over which they are acting.

These stresses are indicated in the following figure.

16
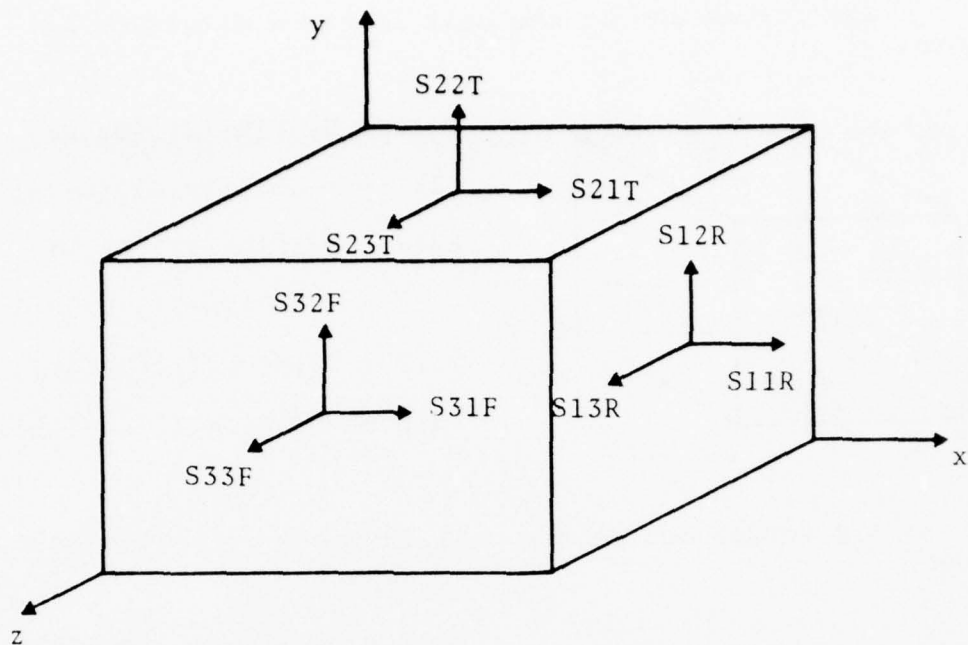
    In addition to the nine stresses as shown, there are
three on the left, three on the back and three on the
bottom side of the cell, a total of 18 stresses.

    There are six forces acting on the cell in the y
direction as shown.
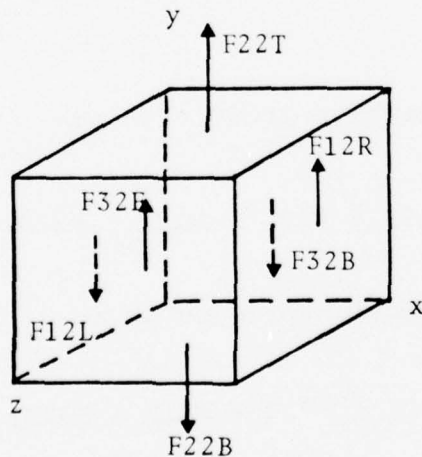
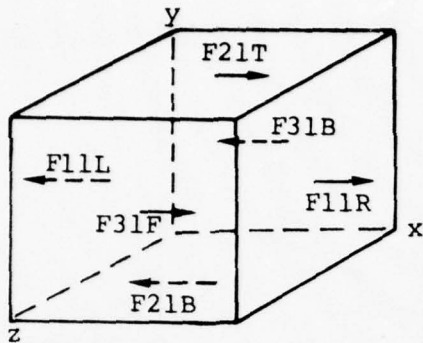$$F22T = S22T(Dx(I))(Dz(K))$$

$$F22B = -S22B(Dx(I))(Dz(K))$$

$$F12R = S12R(Dy(J))(Dz(K))$$

$$F12L = -S12L(Dy(J))(Dz(K))$$

$$F32F = S32F(Dx(I))(Dy(J))$$

$$F32B = -S32B(Dx(I))(Dy(J))$$

Six forces act on the cell in the x direction as shown.

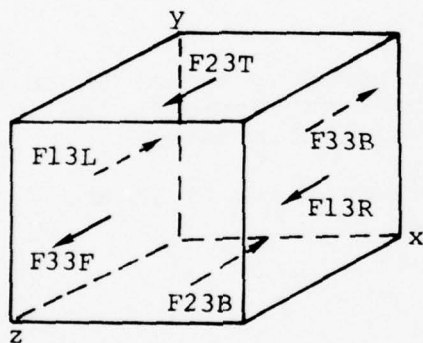$$F11R = S11R(Dy(J))(Dz(K))$$

$$F11L = - S11L(Dy(J))(Dz(K))$$

$$F21T = S21T(Dx(I))(Dz(K))$$

$$F21B = -S21B(Dx(I))(Dz(K))$$

$$F31F = S31F(Dx(I))(Dy(J))$$

$$F31B = -S31B(Dx(I))(Dy(J))$$

Six forces act on the cell in the z direction as shown.

$$F33F = S33F(Dx(I))(Dy(J))$$

$$F33B = -S33B(Dx(I))(Dy(J))$$

$$F13R = S13R(Dy(J))(Dz(K))$$

$$F13L = -S13L(Dy(J))(Dz(K))$$

$$F23T = S23T(Dx(I))(Dz(K))$$

$$F23B = -S23B(Dx(I))(Dz(K))$$

The six forces in the z direction produce an acceleration of

$$\frac{dw}{dt} = \frac{1}{M_{(L)}} [F33F + F33B + F13R + R13L + F23T + F23B].$$

The six forces in the x direction produce an acceleration of

$$\frac{du}{dt} = \frac{1}{M_{(L)}} [F11R + F11L + F21T + F21B + F31F + F31B]$$

18

and the six forces in the y direction produce an accelera-
tion of

$$\frac{dv}{dt} = \frac{1}{M_{(L)}} [F22T + F22B + F12R + F12L + F32F + F32B] \ .$$

These 18 forces will do work such that

$$\rho \ \frac{\partial E}{\partial t} = (\sigma_{ij} \ u_i)_{i,j}$$

or

$$M_{(L)} \ \frac{\partial}{\partial t} \left[I_{(L)} + \frac{1}{2} [u^2_{(L)} + v^2_{(L)} + w^2_{(L)}] \right]$$

$$= \{F11R(UR) + F11L(ULL) + F21T(UA) + F21B(UB)$$

$$+ F31F(UF) + F31B(UBA) + F22T(VA)$$

$$+ F22B(VB) + F12R(VR) + F12L(VLL)$$

$$+ F32F(VF) + F32B(VBA) + F33F(WF)$$

$$+ F33B(WBA) + F13R(WR) + F13L(WLL)$$

$$+ F23T(WA) + F23B(WB) \} = \Delta E$$

or

$$\Delta Q_{(L)} = \frac{\Delta t}{M_{(L)}}(\Delta E) - \left[u_{(L)} \Delta u_{(L)} + v_{(L)} \Delta v_{(L)} + w_{(L)} \Delta w_{(L)} \right.$$

$$\left. + \frac{\Delta u_{(L)}^2 + \Delta v_{(L)}^2 + \Delta w_{(L)}^2}{2} \right]$$

19

where the u, v and w are Phase 1 velocities and the velocity multiplying the stress is an average velocity (Phase 1) across that particular face at which the stress is applied. This requires the saving of columns and slabs of u, v and w velocities from Phase 1.

One requires only to solve for the stresses at the top, right and front of each cell, since the stresses have been calculated at the bottom (from the previous row), at the left (from the previous column sweep) and at the back (from the previous slab sweep).
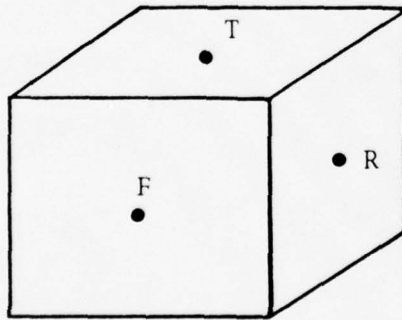
The stresses at the right (R) side of the cell (see the figure below) are

$$\sigma_{ij} = B\left(\dot{e}_{ij} - \frac{\delta_{ij}}{3}\,\dot{e}_{aa}\right)$$

where

$$B = \left(\frac{2y^2}{\dot{\varepsilon}_{ab}\,\dot{\varepsilon}_{ab}}\right)^{1/2}$$ (y is defined on page 22)

On the right side (R), the stresses are

$$S11R = BR\left[\frac{\partial u}{\partial x} - \frac{1}{3}\left(\frac{\partial u}{\partial x} + \frac{\partial v}{\partial y} + \frac{\partial w}{\partial z}\right)\right]$$

$$S12R = \frac{BR}{2}\left[\frac{\partial u}{\partial y} + \frac{\partial v}{\partial x}\right]$$

$$S13R = \frac{BR}{2}\left[\frac{\partial u}{\partial z} + \frac{\partial w}{\partial x}\right]$$

20

On the top side (T), the stresses are

$$S22T = BT\left[\frac{\partial v}{\partial y} - \frac{1}{3}\left(\frac{\partial u}{\partial x} + \frac{\partial v}{\partial y} + \frac{\partial w}{\partial z}\right)\right]$$

$$S21T = \frac{BT}{2}\left[\frac{\partial v}{\partial x} + \frac{\partial u}{\partial y}\right]$$

$$S23T = \frac{BT}{2}\left[\frac{\partial v}{\partial z} + \frac{\partial w}{\partial y}\right]$$

On the front side (F), the stresses are

$$S33F = BF\left[\frac{\partial w}{\partial z} - \frac{1}{3}\left(\frac{\partial u}{\partial x} + \frac{\partial v}{\partial y} + \frac{\partial w}{\partial z}\right)\right]$$

$$S32F = \frac{BF}{2}\left[\frac{\partial w}{\partial y} + \frac{\partial v}{\partial z}\right]$$

$$S31F = \frac{BF}{2}\left[\frac{\partial w}{\partial x} + \frac{\partial u}{\partial z}\right]$$

The velocity gradients and the second strain rate tensor $\dot{\varepsilon}_{ab}\,\dot{\varepsilon}_{ab}$ are all calculated at the three positions indicated and the velocities are the tilda ($\tilde{\ }$) Phase 1 velocities.

Provisions exist for subcycling this strength routine. The Δt for each subcycle is not $\Delta t_H/N$ (where Δt_H is the hydrodynamic time step) but is calculated as follows:

$$\Delta t_H \frac{(N2+1-N)\,2}{N2\,(N2+1)}$$

21

where N2 = number of subcycles and N is the particular subcycle.

The yield strength in simple shear is considered to be a function of pressure and energy and is calculated as

$$Y = (Y_0 + \alpha P)(1 - Q/Q_M)$$

where

Y_0 = yield strength, jerks/cm^3

α = constant

Q_M = energy to melt, jerks/g .

The rigid plastic equations are only applied to those zones that have a $\rho/\rho_0 > 1.0$ or if $\rho/\rho_0 < 1.0$ and $Q > Q_I$ (Q_I is an input number).

Those cells, in which the original velocity has not changed by $\sim 5\%$ are bypassed for the strength calculation (Phase 3).

III.   TWO THREE-DIMENSIONAL IMPACT CALCULATIONS

A comparison between a normal (two-dimensional R-Z) calculation and a normal (x-y-z) calculation has been completed for a normal impact.

An infinite copper jet moving at a velocity of 7.5×10^5 cm/sec impacted an aluminum target of finite thickness. The radius of the jet (for the two-dimensional calculation) was .115 cm, and keeping the same cross-sectional area for the projectile, resulted in a square cross-sectional rod of .204 cm on each side (Figure III-1).

The Tillotson form of the equation of state was used both in DORF and TRIDORF. The two-dimensional calculation was performed using a grid of 45 zones in the radial, and 48 zones in the axial direction. The three-dimensional calculation was performed using a grid of 12 zones in the x direction, 23 zones in the y direction and 12 zones in the z direction. Note, it is only necessary to solve one-fourth of the problem in the three-dimensional mode, because of the two planes of symmetry.

The results are shown (Figure III-2) for the pressure along the axis of symmetry for the two calculations at a time of about .54 μsec. The agreement is very good, considering the very coarse zoning in the three-dimensional grid. Results such as these add to the credibility of the TRIDORF code.

IV.   OBLIQUE IMPACT

Two calculations, using TRIOIL (with strength), were completed several years ago for the Naval Research Laboratory. The configurations were as follows: A plexiglass sphere (R = .3175 cm) impacting at a velocity of 6.1×10^5 cm/sec on a thin plexiglass target of 2.54 cm thickness. The spherical projectile impacted normal (Figure IV-1) and at 45° to the target (Figure IV-2) where the angle is measured between the flight path and the target.

The figures shown are for the plane of symmetry as a function of time. The sequence begins at the upper left and continues downward. The problem (normal) was rezoned (as indicated on the t = 1.68 μsec figure).

A series of four oblique impacts have been performed using the TRIDORF code. The four calculations involved a copper jet (R = .1 cm) impacting a thin steel target of 1.27 cm thickness. The copper jet was treated as a copper rod with a rectangular cross section (.1772 cm on each side). The impact velocity in all cases was chosen as 7.55×10^5 cm/sec.

Massless tracer particles were placed in an orthogonal grid within the steel plate and copper rod. The configurations at various times and for various planes are shown in Figures IV-3, IV-4, IV-5 and IV-6.

Figure IV-3 is a display of the interaction for the 30° impact problem. The cross-sectional display begins in the upper left, proceeding downwards, for the Z planes (coming out of the paper). The jaggedness of the top surface of the target is due to the large zones used in the calculation. Fine zones were placed in all three directions near the original target-projectile interface.

Figure IV-4 is a similar display for the 45° interaction. Figure IV-5 displays, in addition to the Z values, the interaction (plane of symmetry) as a function of time. The Z planes are displayed for every other Z value. These results are for the 60° impact.

Figure IV-6 is a similar display for the 77.5° impact, as a function of the Z planes. This calculation will require considerably more computer time for complete penetration (if complete penetration will occur).

V. FUEL TARGET INTERACTION

The problem of a copper jet traveling at a velocity of 5.617×10^5 cm/sec penetrating a cylindrical tank of fuel (initial density = 1 g/cc) has been completed. A modified continuous boundary condition at the bottom of the tank allowed the copper jet to continue through the tank at a constant velocity. The copper jet was treated as a rigid body, while the fuel was treated as compressible, using an

24

equation of state developed by John Dienes[5]. The form of
the equation of state is

$$P = A\phi + B\phi^3 , \quad \text{where } \phi = \log(\rho/\rho_0) .$$

The calculation (two-dimensional) was carried to a
time of t = 1.84 μsec when the copper jet had penetrated
the top of the cylindrical tank. Stress waves have re-
flected from the top of the tank, but the stress wave has
not reached the upper right corner of the tank at this time.

Subroutines ADJUST and CUBIT were used to rezone the
two-dimensional grid such that the axial and radial zoning
will be identical to the x and y zoning for the three-
dimensional problem. Figure V-1 indicates the initial
configurations for the two- and three-dimensional problems.
The radial pressure at the bottom of the cylindrical tank
is displayed in Figure V-2B. The axial pressures (for given
radial positions) are displayed in Figure V-2A. These re-
sults are at the completion of the two-dimensional calcu-
lation.

Figure V-3A shows density profiles for an early time
(2-D) interaction. One can see the cavitation appearing
along the rigid rod.

Representative pressures (at the completion of the
three-dimensional calculation) are shown in Figures V-3B
and V-3C. Figure V-3B shows pressure contours for the
front face of the three-dimensional configuration. Figure
V-3C shows the pressure contour for the bottom face of the
box. Figure V-4A presents pressure versus distance along
the bottom and top edge of the front face of the cube.
Figure V-4B presents pressure versus time at the top right
hand corner and bottom right hand corner of the front edge
of the box. Additional pressure and velocity profiles
are necessary to complete the flow patterns in the corners
of the box.

---

[5] Dienes, John, "The Response of Gelatin to High Speed
Impact, SSS-IR-74-2120.

25

VI. MULTI-MATERIAL IMPACT

The configuration for the multi-material impact is shown in Figure VI-1.

A copper jet ($R = 1$ mm) impacted on a finite aluminum target (thickness of 3.75 cm) at a velocity of 7.5×10^5 cm/sec. There are 35 zones in the radial direction and 90 zones in the axial direction.

Figure VI-2 shows density plots of the interaction as a function of time. The density plots are produced by assigning ~ 100 random particles to the cell with the largest density. All other cells are then plotted with a number of particles proportional to the cell density divided by the maximum density multiplied by 100.

VII. CODE MODIFICATIONS

Several code modifications were required in order to complete the fuel target interaction problem.

The slug was treated as a rigid body and moved through the grid with a constant velocity. This required modifications in the transport phase and the Lagrangian phase of the DORF code. A continuous bottom boundary condition was required in order to simulate the infinite slug. An artificial viscosity routine (with linear and quadratic terms) was incorporated into the DORF code. The viscosity is calculated at the zone interfaces rather than cell centers. These artificial viscosity terms were then incorporated into the momentum and energy equations for the Lagrangian phase of the calculation.

The two-dimensional calculation for the slug penetration was carried out until the stress wave reached the wall. At this time, the codes ADJUST[3] and CUBIT[3] were used to rezone the problem such that the zoning in the R and Z direction for the two-dimensional results would be identical to the zoning in the X and Y direction for a plane in the three-dimensional grid. One can then transfer the v component of velocity, the specific internal energy and the density directly and transform the u component of velocity from the two-dimensional grid to the u and w components in the three-dimensional grid.

Modifications to the DORF code for interior rigid boundaries have been completed. These interior boundaries must coincide with cell boundaries. A material flag, "9", designates that the 4 sides of the cell are to be treated as reflective boundaries. Options of allowing the bottom, top and right side of the computational grid to be either reflective or transmittive have been added. The sound speed for the Tillotson formulation of the equation of state has been changed to perform the evaluation of the analytical form of

$$ c^2 = \left.\frac{\partial P}{\partial \rho}\right|_Q + \left.\frac{\partial P}{\partial Q}\right|_\rho \frac{P}{\rho^2} \quad . $$

Basic equations for a splitting version of the OIL code have been derived. In addition, the conventional "if" tests have been removed and replaced with functions whose values are 0 or 1.0. The splitting technique and the removal of the conventional "if" tests are applicable to the new generation of parallel and vector computers.

ACKNOWLEDGMENTS
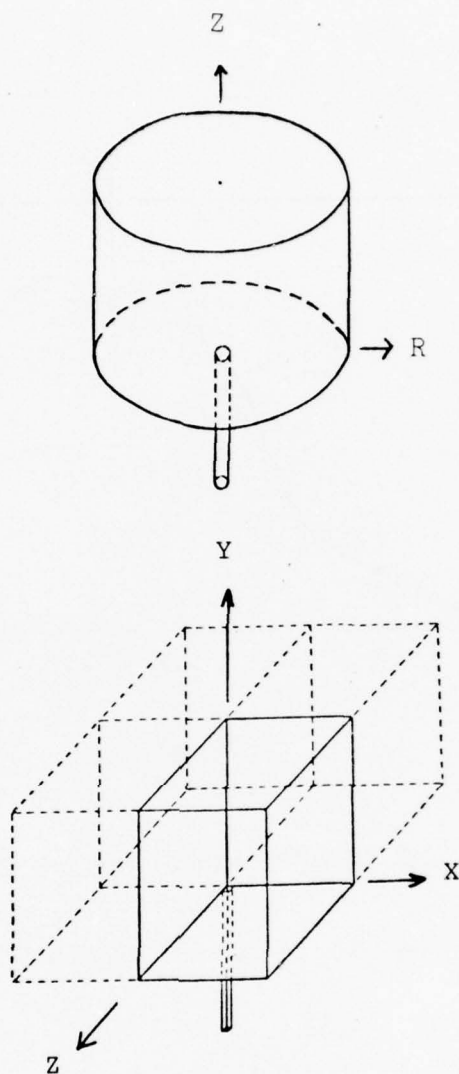
Figure III-1.   2D - 3D   Initial Configuration for Normal
                Impact
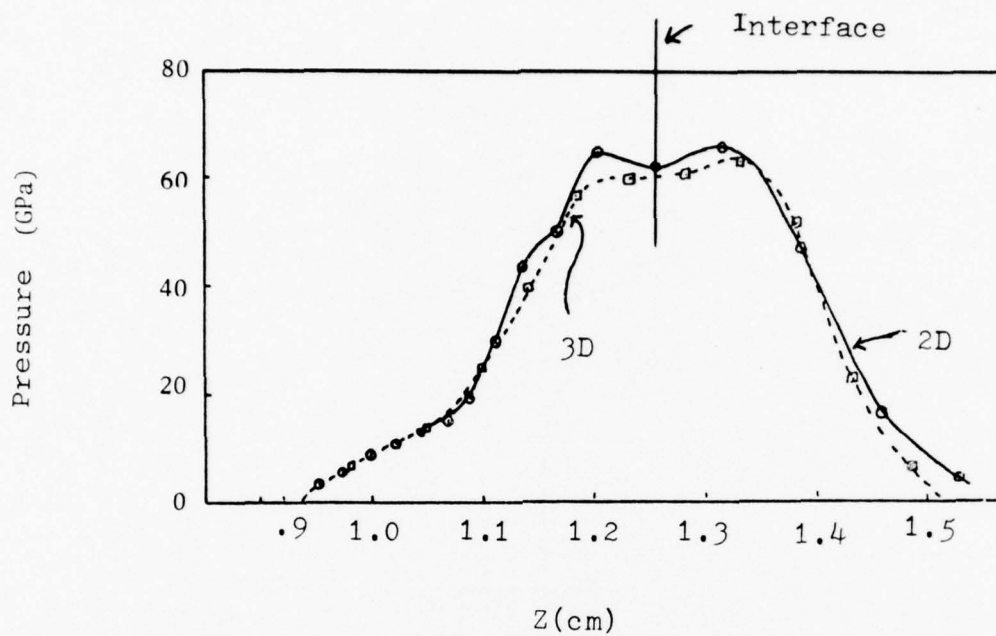
Figure III-2. Pressure Versus Distance (into Target) for
2D - 3D

30

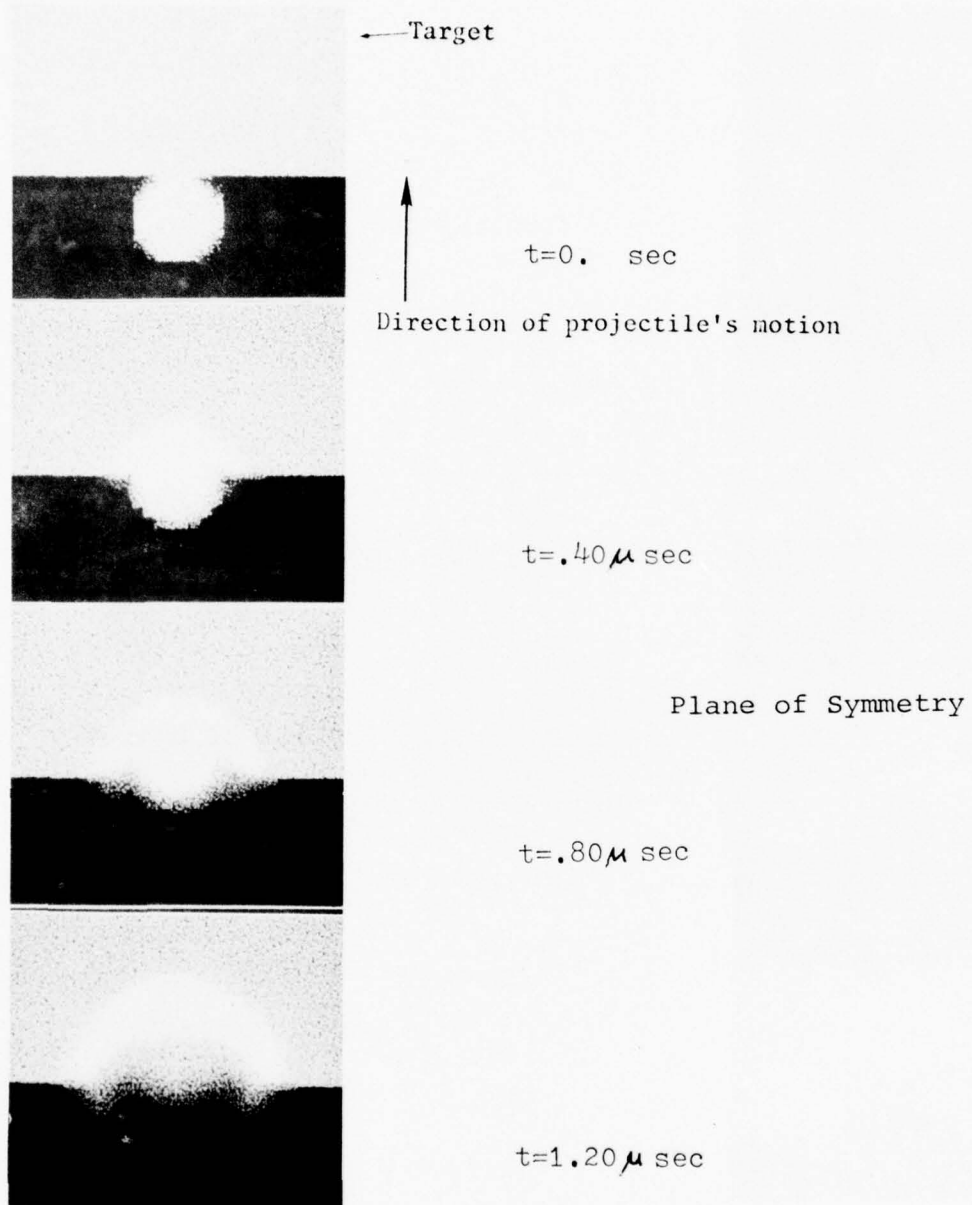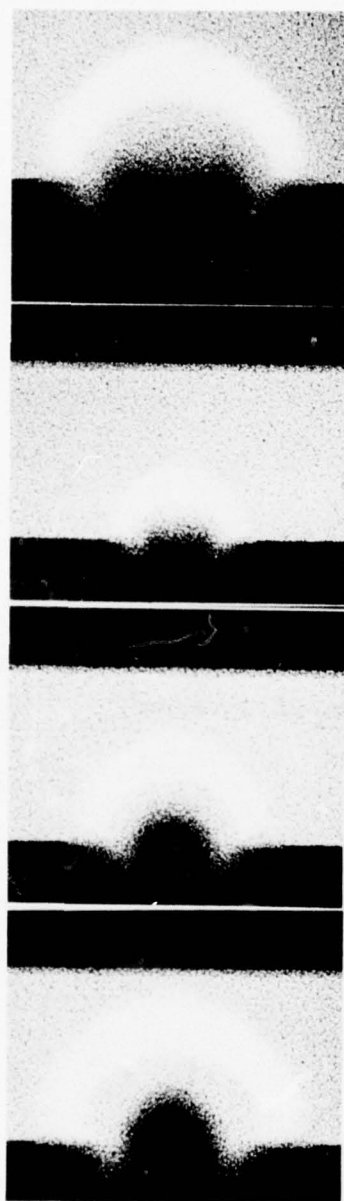Figure IV-1. Density as a Function of Time for the Normal Impact

31

t=1.45 μ sec

t=1.68 μ sec (Grid rezoned)

Plane of Symmetry

t=3.18 μ sec

t=4.5 μ sec

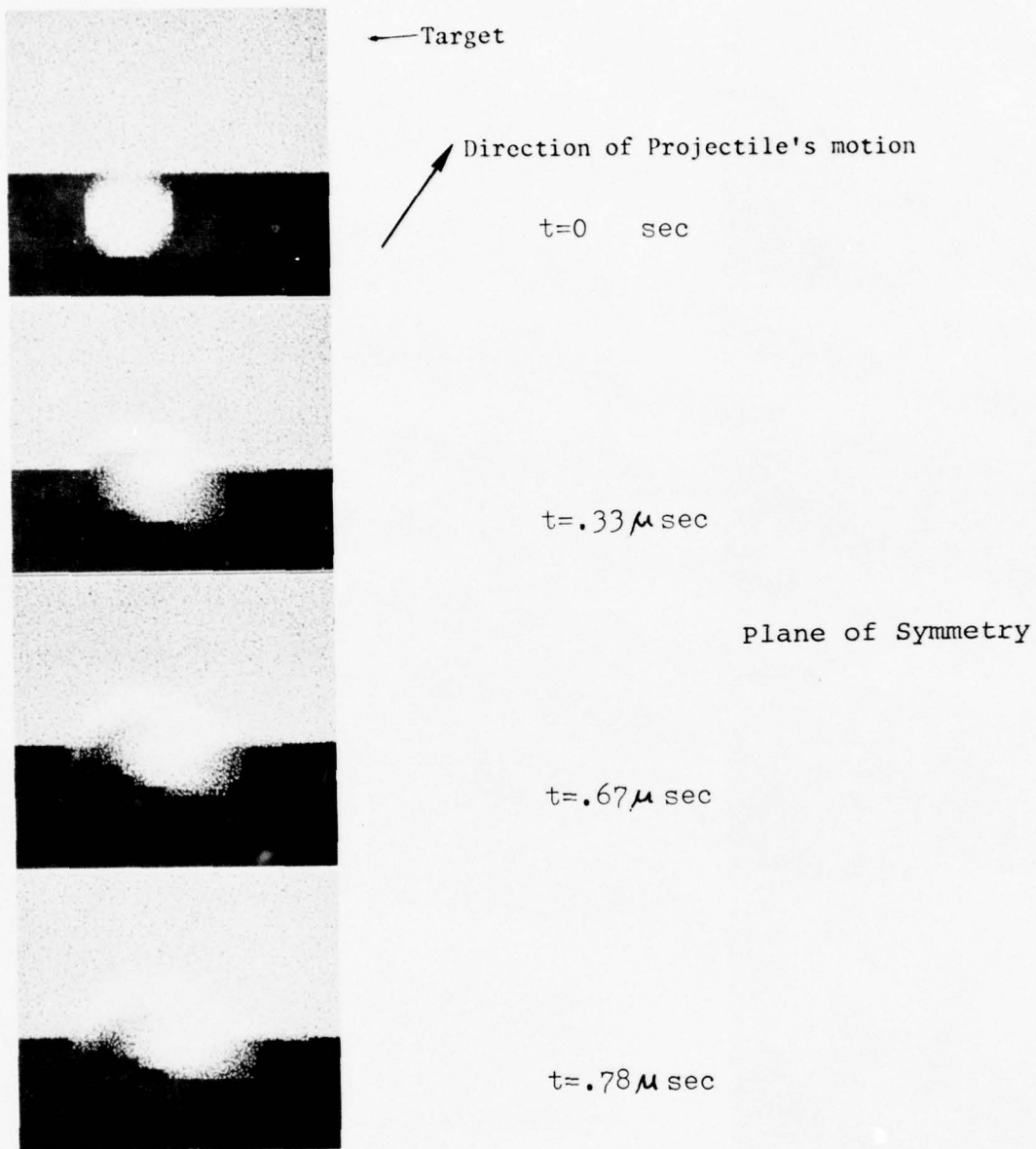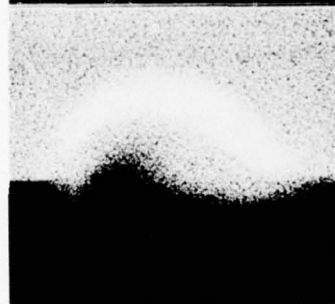Figure IV-1.   Density as a Function of Time for the Normal
Impact (continued)

32

Figure IV-2. Density as a Function of Time for the 45°
Impact

t=.90μ sec

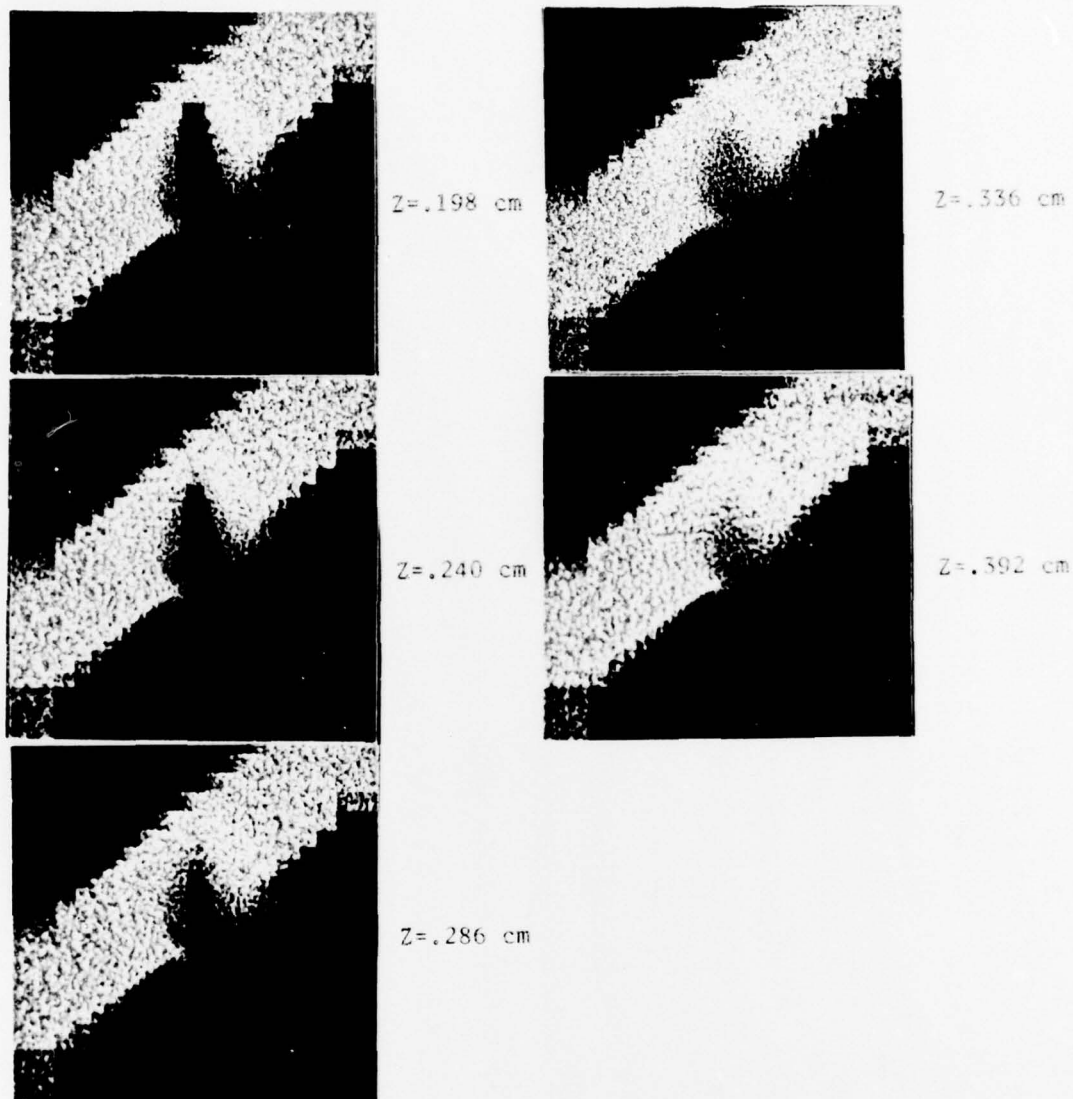t=1.15μ sec

Plane of Symmetry

t=1.40μ sec
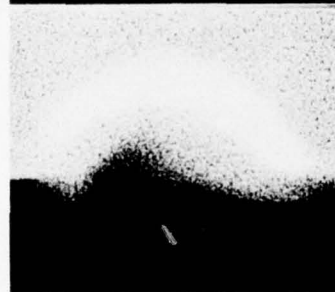
t=1.7μ sec

Figure IV-2.   Density as a Function of Time for the 45°
              Impact (continued)
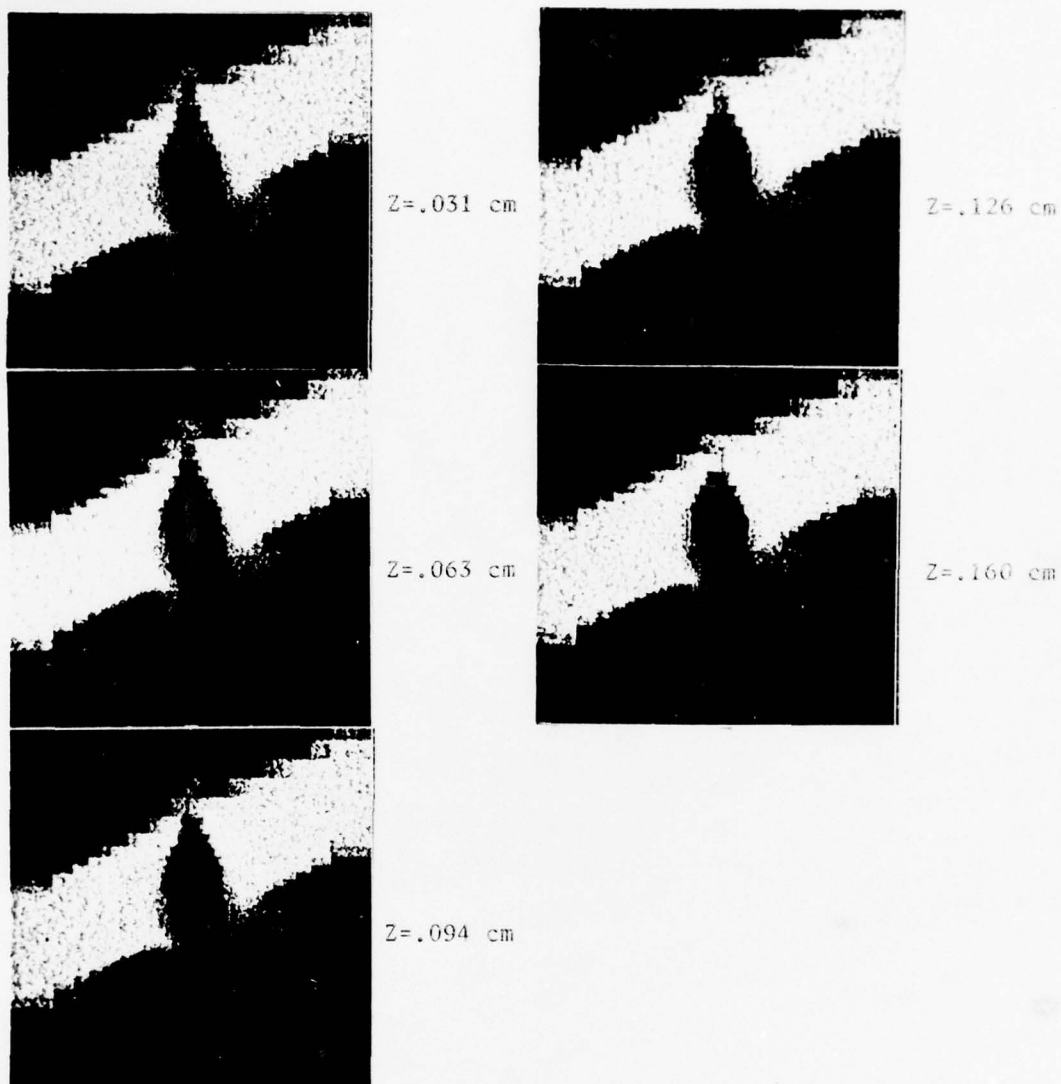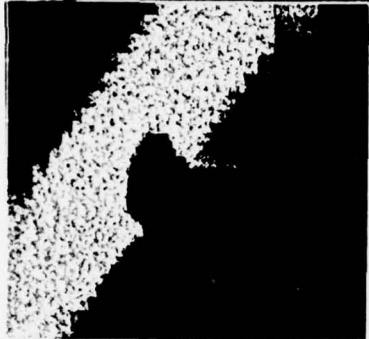
34

Z=.031 cm

Z=.126 cm

Z=.063 cm

Z=.160 cm

Z=.094 cm

Figure IV-3. Density as a Function of Z at a Time of 3.57 μsec
for the 30° Impact

35

Z=.198 cm

Z=.336 cm

Z=.240 cm

Z=.392 cm

Z=.286 cm
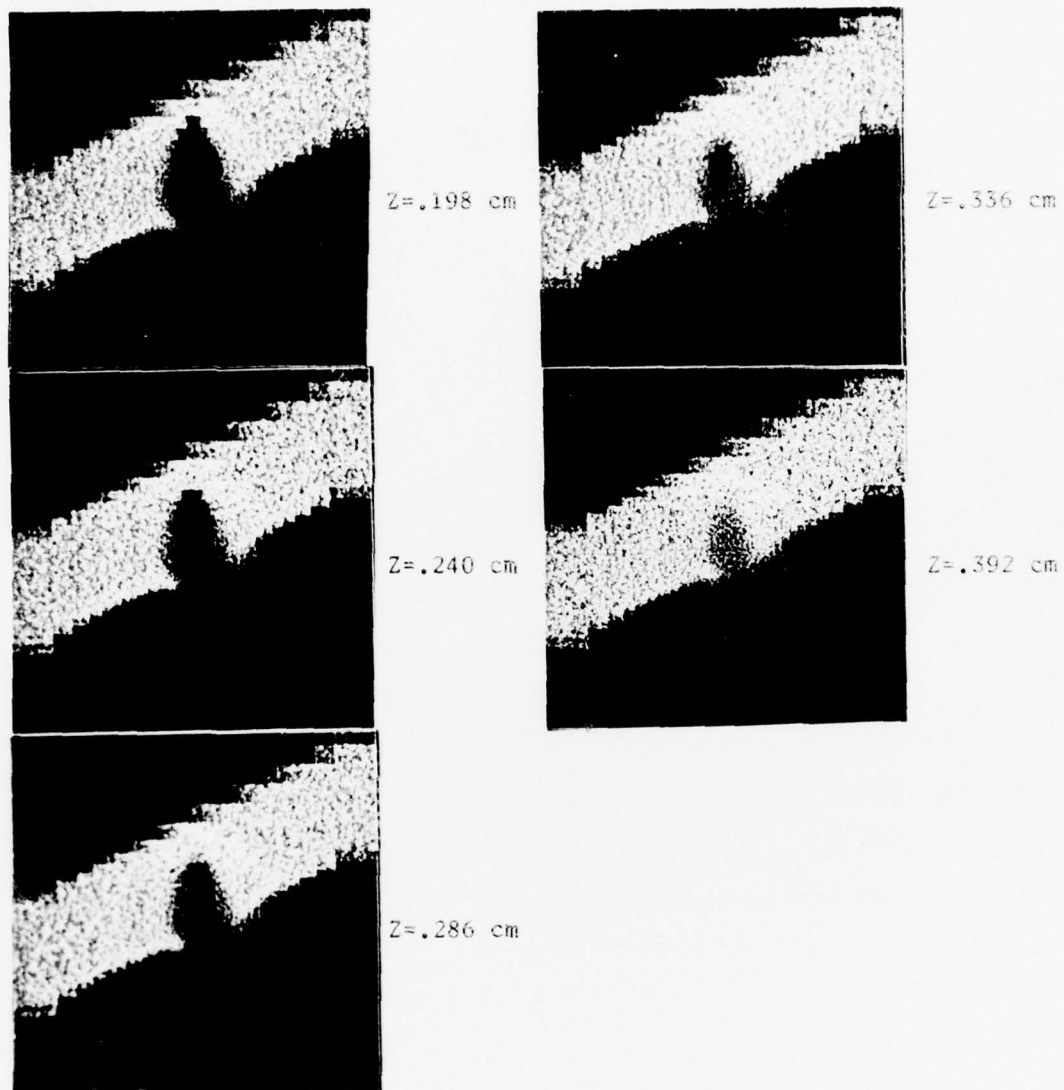
Figure IV-3. Density as a Function of Z at a Time of 3.57 usec
for the 30° Impact (continued)
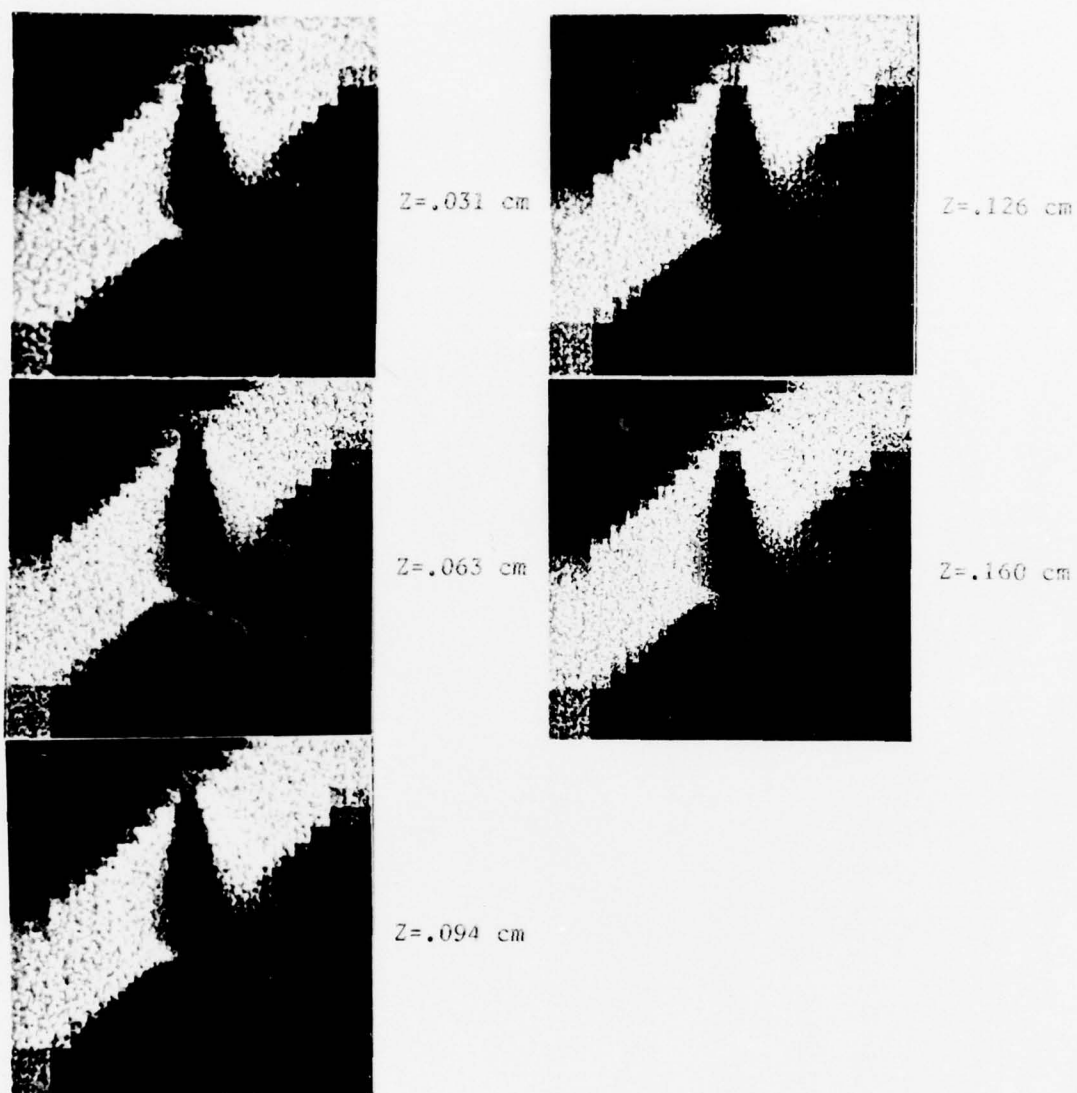
37

Z=.031 cm

Z=.126 cm

Z=.063 cm

Z=.160 cm

Z=.094 cm

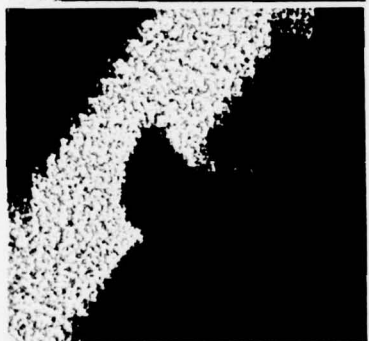Figure IV-4. Density as a Function of Z at a Time of 4.41 usec
for the 45° Impact

39

Z=.198 cm

Z=.336 cm

Z=.240 cm

Z=.392 cm

Z=.286 cm

Figure IV-4. Density as a Function of Z at a Time of 4.41 μsec
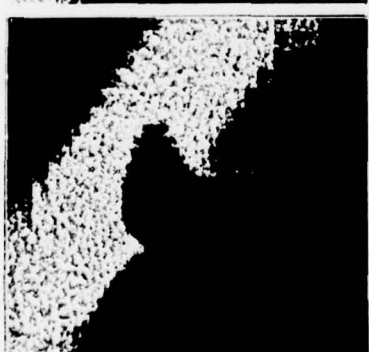for the 45° Impact (continued)

41

t=2.74 µsec

t=3.08 µsec

Z=.031 cm

t=3.46 µsec

t=3.84 µsec

Figure IV-5. Density as a Function of Time and Z for the 60°
Impact

43
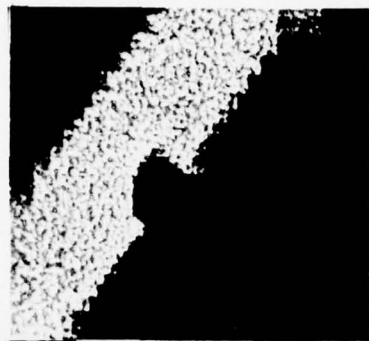
Z=.094 cm

Z=.160 cm

t=3.84 μsec

Z=.240 cm

Z=.336 cm

Figure IV-5. Density as a Function of Time and Z for the 60°
Impact (continued)

45

Z=.031 cm

Z=.126 cm

Z=.063 cm

Z=.160 cm

Z=.094 cm

t=2.67 μsec

Figure IV-6. Density as a Function of Z for the 77.5° Impact

47
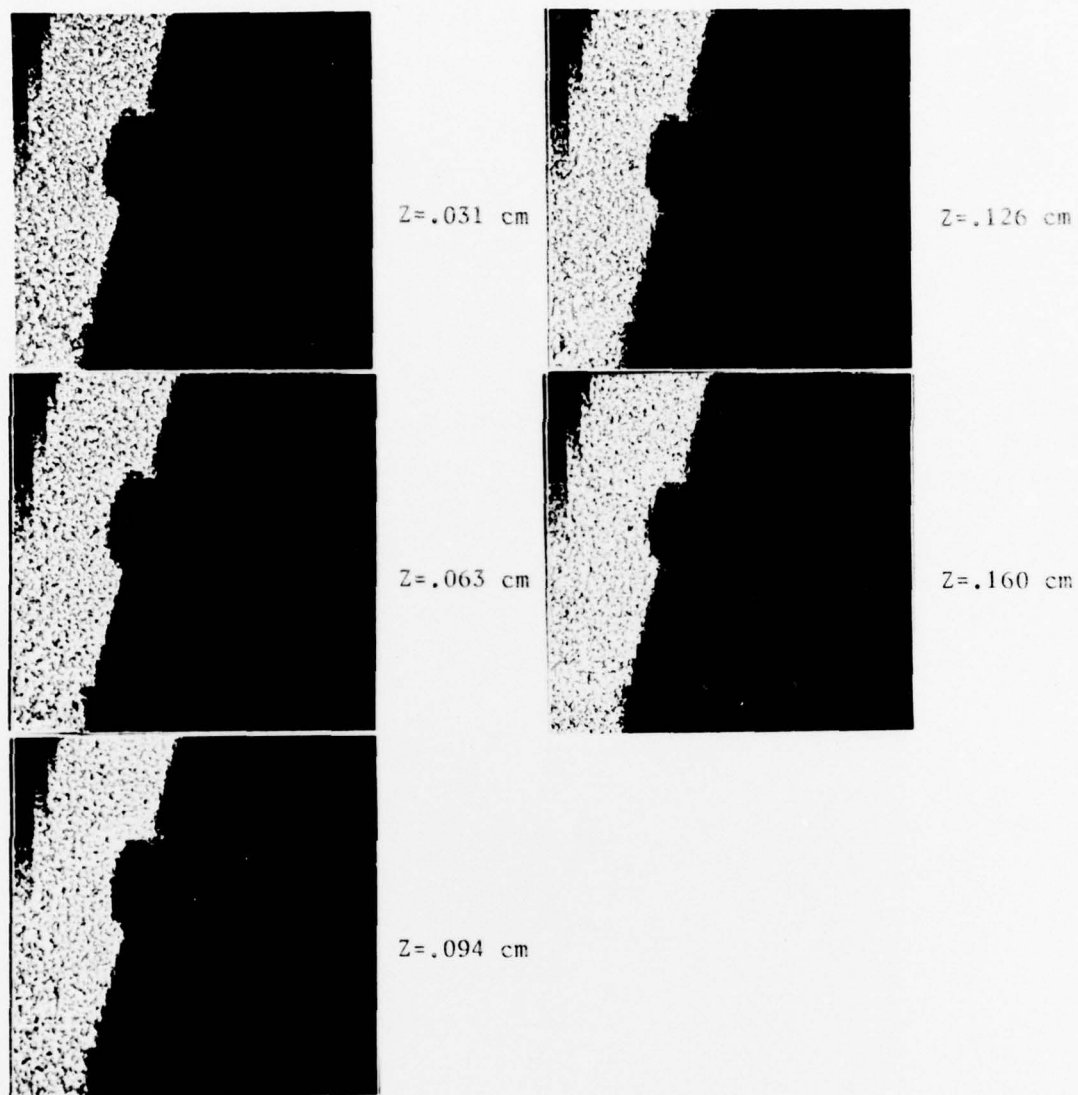
Z=.198 cm

Z=.240 cm

Z=.286 cm

t=2.67 μsec

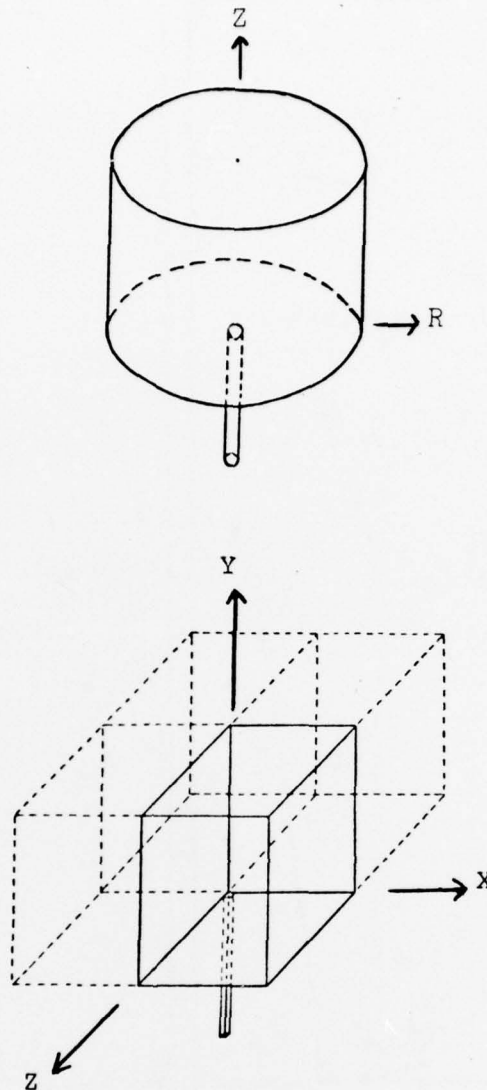Figure IV-6. Density as a Function of Z for the 77.5° Impact
(continued)

49

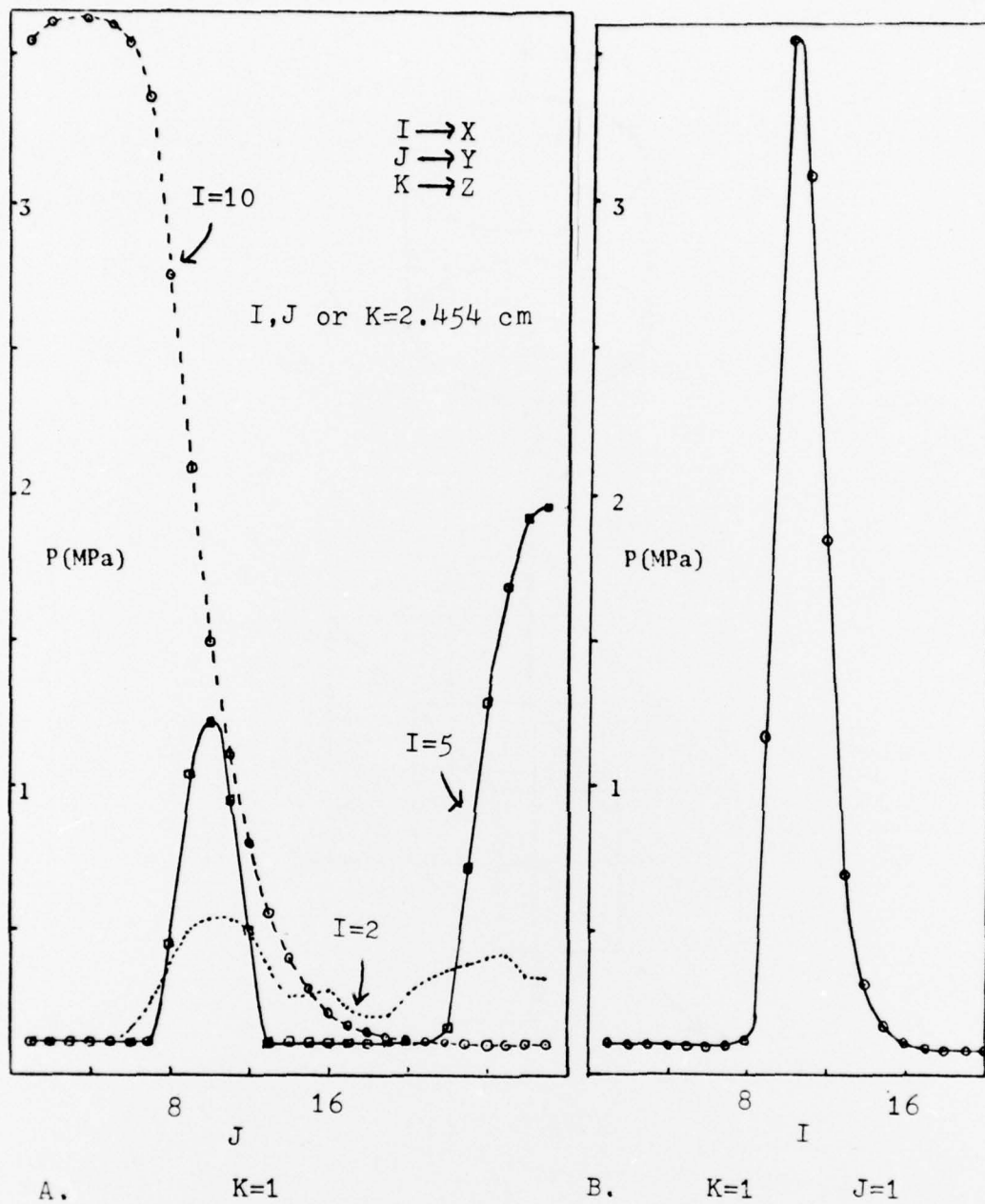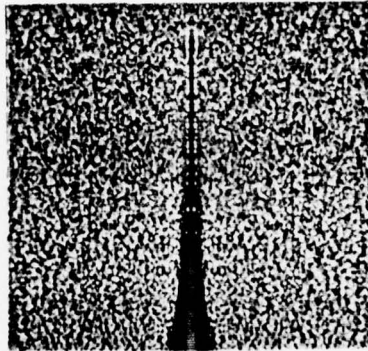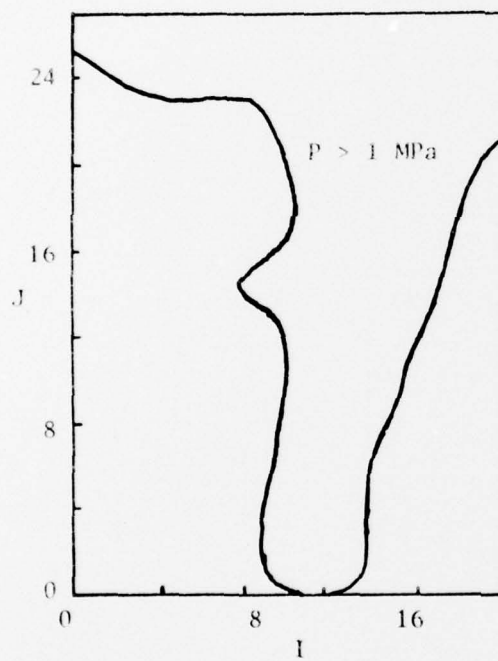Figure V-1.   Initial Fuel Target Interaction (2D - 3D)

51

Figure V-2. Pressures in 3D Mesh at Time of Rezone

A. Early Time Density Distribution (2D)

$P > 1$ MPa

B. Front (K=20)

$P > 1$ MPa
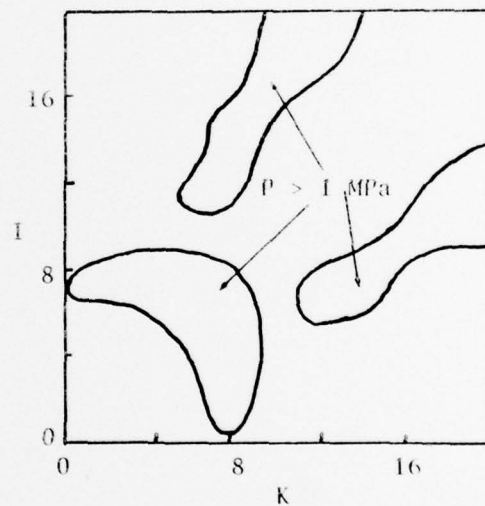
C. Bottom (J=1)

Figure V-3. Pressure Contours at Completion of 3D Calculations

53
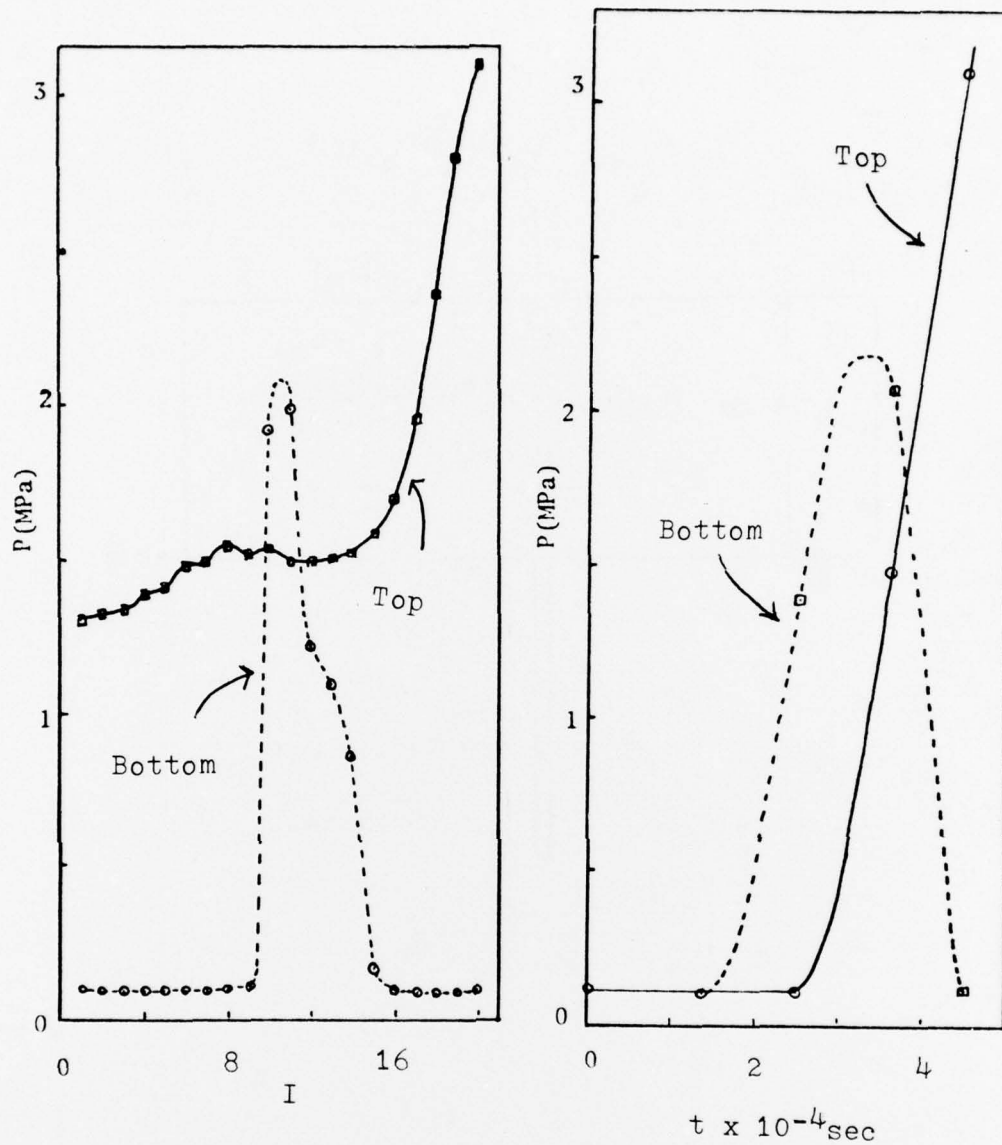
A. K=20

B. Top and Bottom (right corner) for K=20

Figure V-4. Pressure Distribution at Completion of 3D Calculation

55
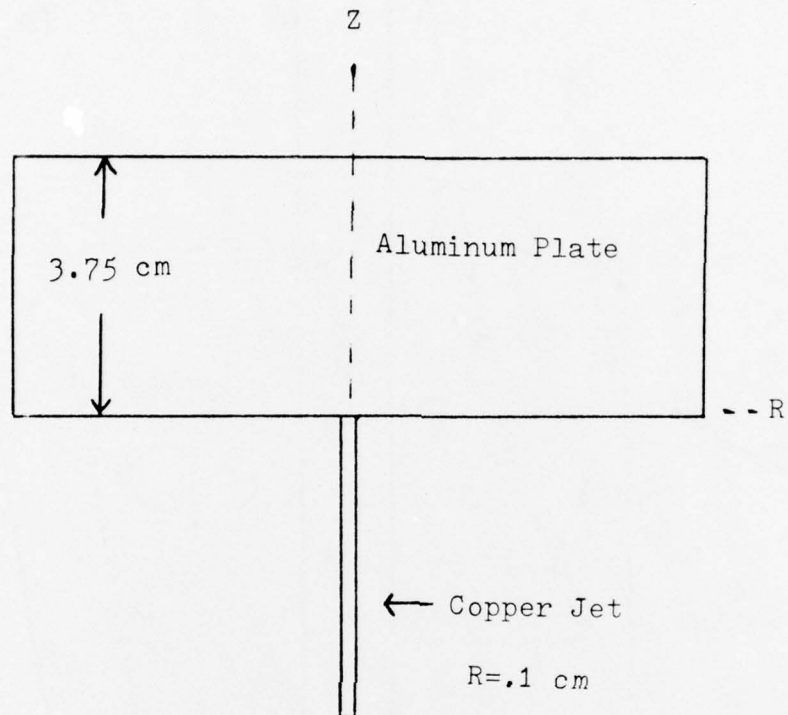
Figure VI-1. Initial Configuration for the Multi-Material
Normal Impact

t=0.00 µsec

t=0.53 µsec

t=1.29 µsec

t=2.10 µsec

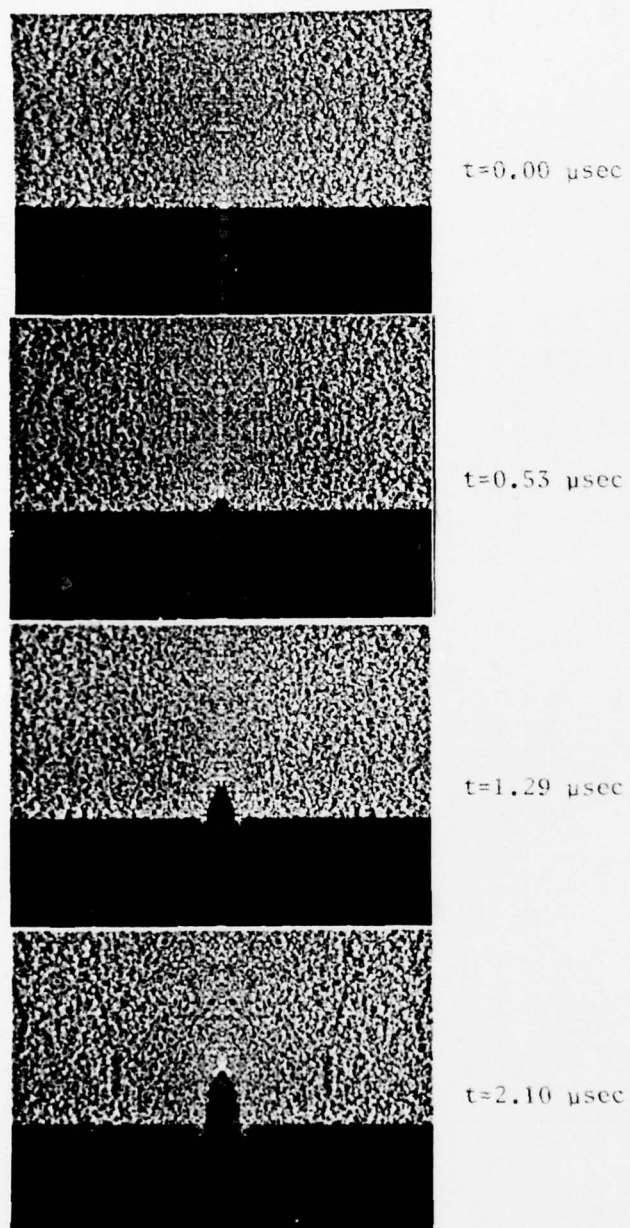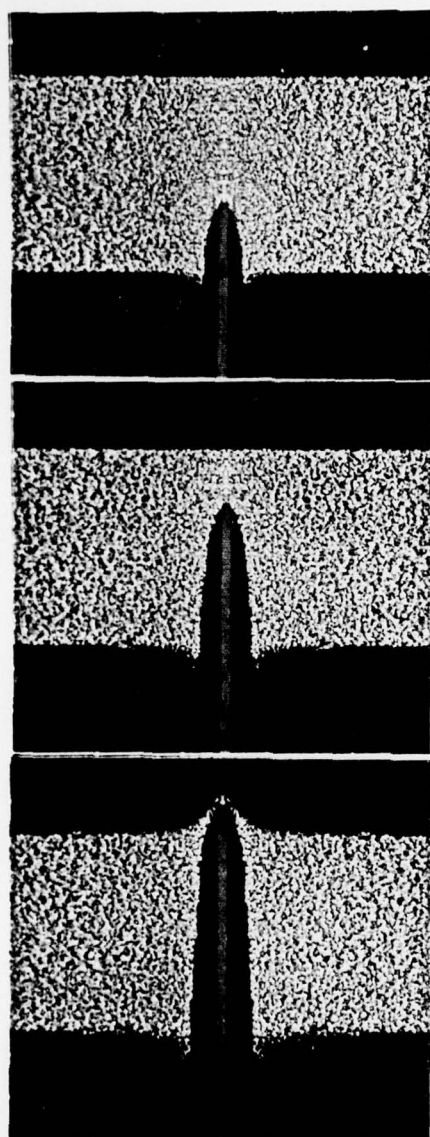Figure VI-2.   Density as a Function of Time for the
Multi-Material Normal Impact

57

t=2.84 µsec

t=5.69 µsec

t=8.85 µsec

Figure VI-2. Density as a Function of Time for the
Multi-Material Normal Impact (continued)

59

DISTRIBUTION LIST

No. of Copies	Organization	No. of Copies	Organization

12 Commander
Defense Documentation Center
ATTN: DDC-TCA
Cameron Station
Alexandria, VA 22314

1 Commander
US Army Materiel Development
and Readiness Command
ATTN: DRCDMA-ST
5001 Eisenhower Avenue
Alexandria, VA 22333

1 Commander
US Army Aviation Systems
Command
ATTN: DRSAV-E
12th and Spruce Streets
St. Louis, MO 63166

1 Director
US Army Air Mobility Research
and Development Laboratory
Ames Research Center
Moffett Field, CA 94035

1 Commander
US Army Electronics Command
ATTN: DRSEL-RD
Fort Monmouth, NJ 07703

1 Commander
US Army Missile Research
and Development Command
ATTN: DRDMI-R
Redstone Arsenal, AL 35809

1 Commander
US Army Tank Automotive
Development Command
ATTN: DRDTA-RWL
Warren, MI 48090

2 Commander
US Army Mobility Equipment
Research & Development Command
ATTN: Tech Docu Cen, Bldg. 315
DRSME-RZT
Fort Belvoir, VA 22060

1 Commander
US Army Armament Materiel
Readiness Command
Rock Island, IL 61202

2 Commander
US Army Armament Research
and Development Command
ATTN: J. Pearson
Tech Lib
Dover, NJ 07801

1 Commander
US Army Harry Diamond Labs
ATTN: DRXDO-TI
2800 Powder Mill Road
Adelphi, MD 20783

1 Commander
US Army Materials and
Mechanics Research Center
ATTN: Tech Lib
Watertown, MA 02172

1 Director
US Army TRADOC Systems
Analysis Activity
ATTN: ATAA-SA
White Sands Missile Range
NM 88002

1 Assistant Secretary of
the Army (R&D)
ATTN: Asst for Research
Washington, DC 20310

DISTRIBUTION LIST

No. of Copies	Organization	No. of Copies	Organization
1	Commander US Army Research Office P. O. Box 12211 Research Triangle Park NC 27709	1	Director Lawrence Radiation Laboratory ATTN: Mr. M. Wilkins P. O. Box 808 Livermore, CA 94550
1	Chief of Naval Research Department of the Navy Washington, DC 20325	1	Director National Aeronautics and Space Administration Langley Research Center Langley Station Hampton, VA 23365
1	Commander US Naval Ordnance Systems Cmd ATTN: Code ORD-0332 Washington, DC 20360		
1	Commander US Naval Surface Weapons Center ATTN: Tech Lib Dahlgren, VA 22448	1	Computer Code Consultants ATTN: Mr. W. Johnson 527 Glencrest Drive Solana Beach, CA 92075
2	Commander US Naval Surface Weapons Center ATTN: Code 730 Lib Silver Spring, MD 20910	1	Sandia Laboratories ATTN: L. Bertholf Albuquerque, NM 87115
		1	Systems, Science & Software ATTN: Dr. R. Sedgwick P. O. Box 1620 La Jolla, CA 92037
1	Commander US Naval Weapons Center ATTN: Code 45, Tech Lib China Lake, CA 93555	1	Drexel Institute of Technology Wave Propagation Research Center ATTN: Prof. P. Chou 32nd & Chestnut Streets Philadelphia, PA 19104
1	Commander US Naval Research Laboratory Washington, DC 20375		
1	US Air Force Academy ATTN: Code FJS-RL (NC) Tech Lib Colorado Springs, CO 80840	2	University of California Los Alamos Scientific Lab ATTN: Tech Lib Dr. J. M. Walsh P. O. Box 1663 Los Alamos, NM 87545
1	AFAL (AVW) Wright-Patterson AFB, OH 45433		Aberdeen Proving Ground
1	AFLC (MMWMC) Wright-Patterson AFB, OH 45433		Marine Corps Ln Ofc Dir, USAMSAA